Green Chemistry

Accepted Manuscript

ROYAL SOCIETY OF CHEMISTRY

www.rsc.org/greenchem

Accelerating the Design of Multi-component Nanocomposite Imprinted Membrane by Integrating a Versatile Metal-Organic Methodology with Mussel-Inspired Secondary Reaction Platform

Yilin Wu[a], *Ming Yan*[b], *Xinlin Liu*[c], *Peng Lv*[b], *Jiuyun Cui*[a], *Minjia Meng*[a], *Jiangdong Dai*[b], *Yongsheng Yan*[a], *Chunxiang Li*[a,*]

[a] *School of Chemistry and Chemical Engineering, Jiangsu University, Zhenjiang 212013, China*

[b] *School of Material Science and Engineering, Jiangsu University, Zhenjiang 212013, China*

[c] *School of Energy and Power Engineering, Jiangsu University, Zhenjiang 212013, China*

*Corresponding Author**

E-mail: w526249292@163.com

Telephone Number: +86 0511-88790683; fax: +86 0511-88791800

Abstract

Efforts to engineer novel membrane materials with enhanced anti-fouling and comprehensive properties as well as highly selective separation abilities are hampered by the lacks of effective imprinted cavities and structure stability. In this work, a novel multi-component metal-organic nanocomposite imprinted membrane (MMO-MIM) has been prepared by integrating a bioinspired metal-organic methodology with the secondary surface sol-gel imprinting technique. The synthesis pathway of MMO-MIM involves two steps: initially, a self-polymerized polydopamine process followed by hydrolysis of ammonium fluotitanate is performed on the surface of PVDF membrane, the surface-initiated sol-gel imprinted procedure is then conducted on the obtained bio-adhesive nano-sized TiO_2 surface system for the fabrication of MMO-MIM. Attributing to the formation of the multilayered membrane structure, stronger fouling resistance and largely enhanced adsorption capacities have been obtained in this case. Meanwhile, the as-prepared MMO-MIM not only exhibits a rapid adsorption dynamics, but also possesses an excellent separation performance ($\beta_{\text{MMO-MIM/MMO-NIM}}$ and $\beta_{\text{m-cresol/2,4-DP}}$ are higher than 2.6 and 4.0, respectively) of templates. In addition, the whole synthesis procedures were conducted in aqueous or ethanol solution at ambient temperature, which was environmental friendly for scaling up without pollution.

Keyword: molecularly imprinted nanocomposite membrane, multi-component metal-organic structure, selective separation, bioinspired secondary reaction platform, m-cresol

Introduction

Development of microporous polymeric membranes capable of consuming lower energy in comparison with traditional separation processes like adsorption and distillation is of considerable interest in material science.[1-4] Despite decades of intense research in the field, some inherent drawbacks of membrane materials such as instability, low selectivity and monotonicity are still limiting their development and further applications in industrial. Capable composite membrane materials, with the enhanced flux, better anti-fouling properties, and more recently, selective separation ability have been urgently needed to meet different needs. [5-7] For decades, the efforts to optimize the comprehensive properties of composite membrane materials have been approached mainly through chemical grafting, surface modification, physical blending, and so on. Among various modification strategies, a facile and versatile method that grafting inorganic metal nano-materials onto the membrane surfaces has attracted increasing attention, driven primarily by its relatively facile processing and foreseeable separation performance.[8-12] Although many approaches had successfully modified the microporous polymeric membranes by inorganic metallic nanoparticles, the typical flux and comprehensive performance loss could still be observed due to the blocked agglomeration of nanoparticles and weak binding force between nano-sized materials and membranes.[13-15] Hence, membranes modified by inorganic metal materials capable of both tightly binding and uniform dispersion on the surface of membranes, which can be regarded as the key factor to obtain high performance membranes, is still facing an urgent challenge.

Inspired from the highly bioadhesive performance of mussel protein, Messersmith and co-workers proposed that dopamine could be regarded as an excellent surface-adherent material for multifunctional coatings of membrane surfaces (Figure S1).[16,17] As is well known, dopamine can polymerize and affix to all kinds of inorganic and organic materials through the generation of strong noncovalent and covalent linkages with surfaces.[18-22] Attributed to this self-polymerization composite technology of dopamine, the tightly bio-adhesive and homodisperse polydopamine (pDA) layers can be stuck on membrane surfaces to form a versatile platform for secondary reactions (such as protein immobilization, cells adhesion, and nanoparticle stabilization).[23-29] Meanwhile, there is reason to believe that the metallic nanoparticles (TiO_2 in this study) with highly chemical stability and anti-fouled properties can be uniformly dispersed and tightly bound

onto the pDA-modified versatile membrane platform.

Because of the intrinsic layered structure, the lower sites accessibility and the inexistence of specific recognition sites of normal nanocomposite membranes, issues such as low-permeability and non-selectivity are still limiting their applications in drug delivery, solid-phase extraction, and chromatographic separation. As a specific recognition system, molecularly imprinted technique (MIT) is a straightforward and well-established technique for the intelligent fabrication of selective recognition sites which are well complementary to the size, shape, and functionality of templates onto synthetic materials.[30-33] Because of the outstanding features such as easy preparation, low-cost, and chemical/mechanical stability, molecularly imprinted polymers (MIPs) play central roles in bioseparation, medical diagnostics, drug delivery, and membrane separation. Molecularly imprinted membranes (MIMs) are the membranes composed of MIPs or containing MIPs.[34] Combination of MIPs into nanocomposite membranes could provide membrane-based specific separation for target molecules. In recent years, porous MIMs with highly diversified pore size, multilayered structure, and specific separation performance have attracted plenty of attention.[35-38] However, issues such as high diffusion barrier, low regenerability, poor perm-selectivity, and reduced structure resistance still exist.[39] Herein, a bioinspired multilayered metal-organic structure is developed for the preparation of the high-efficiency MIMs.

In this work, we present a bio-functionalized multilayered metal-organic strategy for developing molecularly imprinted nanocomposite membranes with diversified structures, excellent specific separation property and high regenerability. The phenolic compound from the neutral oils, m-cresol (mainly obtained from petroleum products),[39-46] is used as template molecule. Inspired by the self-polymerization composite performance of dopamine, the synthesis pathway involves prior grafting of pDA layers onto the surface of polyvinylidene fluoride (PVDF) membrane, followed by a hydrolysis process of ammonium fluotitanate. And then a surface-initiated sol-gel imprinted polymerization process is conducted on the bio-functionalized surface, which directs the synthesis of the multilayered metal-organic molecularly imprinted nanocomposite membrane (MMO-MIM). As evidenced in this study, this novel bio-functionalized multilayered membrane structure can not only largely improve the comprehensive performance of MIMs, but also enhance the adsorption capacity, perm-selectivity property, and reinforce the regeneration stability. That is to say, this method could work very well for selective separation and purification of m-cresol in a

complex system. In addition, the whole synthesis procedures were conducted at ambient temperature in aqueous or ethanol solutions, which is easy to scale up at a low cost without pollution.

Experimental

Chemicals

Commercial PVDF powder was purchased from French company Arkema. Ammonia solution (28%-30%), tris (hydroxymethyl) aminomethane (Tris-HCl, 99%), dopamine (98%), 3-aminopropyltriethoxysilane (APTES, 99%), ammonium fluotitanate ($(NH_4)_2TiF_6$), m-cresol (99%) p-cresol (98%), 2,4-dichlorophenol (2,4-DP, 98%), and polyvinylpyrrolidone (PVP) were obtained from Aladdin Reagent Co., Ltd. and used as received (Shanghai, China). Bovine serum albumin (BSA, M_n=68000), tetraethyl orthosilicate (TEOS, 98%), and n-methyl pyrrolidone (NMP) were obtained from Sinopharm Chemical Reagent Co., Ltd. (Shanghai, China). The phosphate-buffered saline (PBS, 0.1 M, pH 7.4) was prepared by the addition of prepackaged buffer salts (Aldrich) to deionized water. Doubly distilled water was used in all cleaning processes and aqueous solutions.

Characterizations of membranes with different surface modifications

The morphological evolutions of various membranes were observed by a field emission scanning electron microscopy (SEM, S-4800). The surface chemical compositions of membranes with different surface modifications were further investigated by the X-ray photoelectron spectroscopy (XPS) measurement with an Omicron ESCA probe spectrometer. The pressure in the analysis chamber was maintained at 5.0×10^{-8} Torr or lower during each measurement. The static water contact angles of various membrane surfaces were measured by the contact angle detecting process. High performance liquid chromatography (HPLC) (Agilent 1200 series, U.S.A.) was used for the determination of m-cresol, p-cresol, and 2,4-dichlorophenol. Detailed determined requirements were shown in Support Information.

Synthesis of pristine PVDF membrane followed by the self-polymerization composite process of dopamine

In a typical PVDF membrane synthesis, 4 g PVDF powder and 21 g NMP were intensive

mixed used as the casting solution of pristine PVDF membrane. PVP in this research was used for getting basement membranes with appropriate pore sizes for further modifications. In order to remove the air bubbles and form a homo-disperse solution, the as-prepared casting solution was sealed under persistently mechanically stirring for 12 h at 50 ^{o}C, and then was sealed and stored for another 24 h at 50 ^{o}C. After that, the as-prepared mixture was cast on a glass plate using a doctor knife. And then the casting solution on the glass substrate was instantly immersed into a coagulant bath containing pure water to undergo a phase inversion. Upon complete coagulation, the as-cast membranes were put into deionized water for solvent-exchange process. After that, the as-prepared pristine membranes were stored in deionized water before use. Subsequently, in a typical pDA modified PVDF membrane (pDA@PVDF) synthesis, first, one piece of pristine PVDF membrane (40 mm in diameter) was dipped into 50 mL 10 mM Tris-HCl (pH=8.5) aqueous solution for 5 min. Second, dopamine (100 mg) was added to above solution to start the self-polymerization procedure. The self-polymerization process was lasting for 6 h under persistently mechanically oscillation at room temperature, and then the pDA-based thin layers could be achieved on the membrane surfaces. Finally, pDA modified PVDF membrane (pDA@PVDF) was obtained after being rinsed with deionized water to wash out redundant pDA particles and unreacted dopamine.

Synthesis of nano-sized TiO_2 layers modified pDA@PVDF followed by the surface-initiated sol-gel imprinted polymerization process with TEOS

The nano-sized TiO_2 layers modified procedure of pDA@PVDF was conducted by the hydrolysis process of ammonium fluotitanate. Typically, one piece of pDA@PVDF was dipped into 300 mM H_3BO_3 aqueous solution for 60 s at room temperature and then immersed in a fresh aqueous solution containing 100 mM $(NH_4)_2TiF_6$ and 300 mM H_3BO_3 (pH=3.86) for 60 min. After the stipulated binding time, the as-prepared TiO_2 modified pDA@PVDF (TiO_2-pDA@PVDF) was washed with abundant deionized water to remove unmodified TiO_2 nanoparticles and then dried in vacuum oven at 30 ^{o}C. Subsequently, the multilayered metal-organic molecularly imprinted nanocomposite membrane (MMO-MIM) was prepared by a surface-initiated sol-gel imprinted polymerization. Typically, 0.5 mmol m-cresol and 0.2 mL APTES were firstly dissolved in 30 mL ethanol for a stirring process for 30 min, after that 0.8 mL TEOS was added to the above solution for another stirring process (the influence of the ratio of APTES/TEOS on the adsorption capacity

of MMO-MIM was investigated in detail, as shown in Figure S2). 0.5 mL of ammonia solution and one piece of the as-prepared TiO_2-pDA@PVDF were then immersed in the above mixture to initiate the imprinted process. The entire surface-initiated sol-gel imprinted polymerization procedure was carried out at room temperature for 12 h in air. After that, the resultant membrane was rinsed with a mixture of ethanol/acetic acid (95:5, v/v) to remove the template molecules and unreacted monomers. Finally, the MMO-MIM was obtained after drying in a vacuum drying chamber. As the control, the multilayered metal-organic non-imprinted nanocomposite membrane (MMO-NIM) was prepared without adding the template molecules and subjected to the same conditions.

BSA adsorption experiments and fouling resistance evaluation

To examine the anti-fouling performance of the pristine and various modified membranes, BSA was used as a model protein to investigate the static and dynamic protein adsorption experiments. The dynamic and static adsorption experiments of BSA onto various membranes were investigated, respectively. The synthesized membrane (40 mm in diameter) was dipped into phosphate buffer (0.1M, pH=7.4) aqueous solution for 5 min and then one piece of filter paper was used for adsorbing the excess buffer solution on the membrane surface. Whereafter, the membrane was fixed into a suitable sealed beaker and then 50 mL of 1mg mL^{-1} BSA aqueous solution (pH=7.4) was added to the beaker. The static adsorption/desorption equilibrium of BSA for various membranes could be obtained after continuing for more than 24 h at room temperature. The adsorption capacities of BSA for different synthesized membranes were calculated from the concentration differences of BSA solutions before and after BSA adsorptions. In addition, the average amount based on the adsorption experiments for different membranes were at least repeated in triplicate. Meanwhile, each dynamic adsorption experiment was performed under vibration process to evaluate the fouling resistance of the pristine, different surface modified membranes, MMO-MIM, and MMO-NIM under simulated “real” condition.

Binding experiments

The binding properties (adsorption kinetics and adsorption isotherm) were measured by the batch mode operations. M-cresol was used as the model molecule to evaluate the binding capacities of MMO-MIM and MMO-NIM. As to the adsorption kinetics experiments, each MMO-MIM (40 mm in diameter) or MMO-NIM was immersed into 10 mL of m-cresol ethanol

solution with the concentration of 600 mg L^{-1}, the supernatant adsorbed solutions were sealed in thermostatic waterbath at 25 ^{o}C and then the resultant solutions were taken out at predetermined time intervals (0, 5.0, 10, 15, 20, 25, 30 min) for the further measurement. For the adsorption isotherm experiments, both MMO-MIM and MMO-NIM were immersed into 20 mL of m-cresol ethanol solutions with different concentrations (50, 100, 200, 400, 600, 800 mg L^{-1}), respectively. And the static adsorption processes were carried out at 25 ^{o}C for 60 min. The adsorption amounts of MMO-MIM and MMO-NIM towards m-cresol were measured by HPLC at 280 nm. The adsorption capacities of MMO-MIM and MMO-NIM could be calculated as follow:

$$Q_t = \frac{(C_0 - C_t)V}{m} \quad (1)$$

$$Q_e = \frac{(C_0 - C_e)\,V}{m} \quad (2)$$

where C_e and C_0 (mg mL^{-1}) represent the initial and equilibrium concentrations, respectively. C_t (mg L^{-1}) is the concentration of m-cresol at different time t. Q_e and Q_t (mg mL^{-1}) represent the adsorption amount of m-cresol. V is the volume of adsorbed solution, m is the molar mass of m-cresol.

To measure the specificity of the as-prepared MMO-MIM and MMO-NIM, the selective static adsorption experiments were studied using m-cresol, p-cresol, and 2,4-DP as the competitive molecules with the initial concentrations of 600 mg L^{-1}. After the selective binding experiments for 60 min, the binding mixtures including m-cresol, p-cresol, and 2,4-DP were measured by HPLC.

Measurement of permeation and perm-selectivity performance

It is critically necessary to investigate the permeation and perm-selectivity performance of MMO-MIM and MMO-NIM, because it provides considerable information about the selective separation mechanism. The permeation tests were performed by an H-model tube installation as shown in Figure S3. As shown, the MMO-MIM or MMO-NIM was mounted on the H-model separation apparatus. In the m-cresol permeation and competitive permeability tests, the permeation fluxes of different targets for MMO-MIM and MMO-NIM were measured by analyzing an aliquot of the solution from the receiving phase by HPLC method. To the most precise information for different modules, each experiment was repeated for three times by the same type of membranes (MMO-MIM or MMO-NIM). In addition, the mixture solutions in both

feeding phase and receiving phase were kept homogeneous by waterbath thermostatic oscillator at 25 °C. The permeation flux J (mg cm^{-1} h^{-1}), the permeability coefficient P (cm^2 h^{-1}) and the permeation factors $\beta_{\text{MMO-MIM/MMO-NIM}}$, $\beta_{\text{m-cresol/2,4-DP}}$ and $\beta_{\text{m-cresol/p-cresol}}$ are calculated as follows:

$$J_i = \frac{\Delta C_i V}{\Delta t A} \qquad i = \text{m-cresol, p-cresol, 2,4-DP} \tag{3}$$

$$P = \frac{J_i d}{(C_{Fi} - C_{Ri})} \qquad i = \text{m-cresol, p-cresol, 2,4-DP} \tag{4}$$

$$\beta_{(MMO-MIM)/(MMO-NIM)} = \frac{P_{MMO-MIM}}{P_{MMO-NIM}} \tag{5}$$

$$\beta_{m-cresol/2,4-DP} = \frac{P_{m-cresol}}{P_{2,4-DP}} \tag{6}$$

$$\beta_{m-cresol/p-cresol} = \frac{P_{m-cresol}}{P_{p-cresol}} \tag{7}$$

where V, A, and d represent the volumes of feeding and receiving phases (mL), effective membrane area (cm^2), and the thickness of membranes, respectively. $\Delta C_i/\Delta t$ is the change of concentration in the receiving solution. (C_{Fi}-C_{Ri}) is the concentration difference between feeding and receiving phases.

Results and discussion

Synthesis pathway to incorporate multilayered metal-organic structure into bio-inspired molecularly imprinted nanocomposite membrane

Herein we propose a strategy for the synthesis of multilayered metal-organic molecularly imprinted nanocomposite membrane (MMO-MIM) with highly dense and accessible specific recognition sites of m-cresol. As illustrated in Figure 1, inspired by the self-polymerization composite ability of dopamine, a tightly bio-adhesive and homodisperse pDA layer could be stuck on the membrane surface.[17,18] Subsequently, the pre-modified pDA@PVDF was further modified by a hydrolysis process of ammonium fluotitanate to robustly bind TiO_2 film on the surface of pDA@PVDF. Attributing to the creation of the bio-functionalized pDA thin layer, the TiO_2 films could be uniformly dispersed and tightly bounded onto the surface of PVDF membranes to form the metal-organic nanocomposite structure (TiO_2-pDA@PVDF).[17,23-25]

This in-situ attraction and formation of TiO_2 can assist the homogenous distribution and the tight binding of TiO_2 nanoparticles onto the membrane surfaces for the potential performance enhancement. Innovation individually, a surface-initiated sol-gel imprinted polymerization

approach was then conducted on the surface of the synthesized TiO_2-pDA@PVDF. In this work, the MMO-MIM was prepared in two steps by firstly the prepolymerization of template molecule m-cresol and functional monomer APTES, and followed by a sol-gel polymerization with TEOS initiated by ammonia solution. In addition, the whole imprinted procedure was carried out in ethanol solution which was environmental friendly. Meanwhile, this strategy enables the imprinted sites to situate onto the surfaces or in the proximity of PVDF membranes' surfaces, so that, nearly all the imprinted cavities are accessible to template molecules and fast dissociation/association kinetics and special separation performance could be obtained (Figure 1). Meanwhile, the approach reported here consists of several straightforward and environment-friendly processes, directing it as a promising candidate for large-scale application in specific molecule recognition, separation, biosensors, and so on.

Physicochemical characterizations of various membranes and MMO-MIM

The deposition of pDA, hydrolysis process of ammonium fluotitanate, and the sol-gel imprinting process on the membrane surfaces are confirmed by X-ray photoelectron spectroscopy (XPS). According to the XPS wide spectra of pristine PVDF and pDA@PVDF (Figure 2), pDA@PVDF displays the new peaks of N1s and O1s peaks, which implies the readily deposition of pDA layer on pristine PVDF membrane. In addition, Fourier Transform infrared spectroscopy (FTIR) was used to further analyze the surface composition of pristine PVDF and pDA@PVDF, as shown in Figure S4, compared with the pristine PVDF, the pDA@PVDF shows several new absorption signals. The peaks at 1550 cm^{-1} and 1650 cm^{-1} are attributed to the N-H bending vibrations and the C=C resonance vibrations, respectively. The broad absorbance between 3700 and 3000 cm^{-} is ascribed to O-H/N-H stretching vibrations. Also these results strongly indicate the successful modification of pDA on the membrane surfaces.

After the hydrolysis process of ammonium fluotitanate, the Ti peak shows up, suggesting the formation of TiO_2 films on the surface of pDA@PVDF. Finally, as shown in the wide spectra of MMO-MIM in Figure 2, the F1s peak from the PVDF support is almost shielded and the Ti2p peak is completely shielded. Instead, the intensity of O1s peak enhances, and the new peaks of Si2s and Si2p can be observed, indicating the synthesis of MMO-MIM after the sol-gel imprinting procedure. As shown in Figure 3, on the narrow scan for N1s (A) peak of pDA@PVDF, the C-N and N-H peaks also strongly verify the successful deposition of pDA layer on the pristine PVDF

membrane.[24] Then, as shown on the narrow scan for Ti2p (B) of TiO_2-pDA@PVDF, the peaks of Ti2p 3/2 and Ti2p 1/2 indicate the normal state of Ti^{4+} in the TiO_2, which demonstrate the binding of TiO_2 layer onto pDA@PVDF.[47-51] And the emerging peaks of Si-O and Si-C on the narrow scan for Si2p (C) of MMO-MIM fully testify the formation of imprinting layer according to the sol-gel process on the surface of PVDF membrane. In addition, Figure 3D and 3F describe the curve-fitting results for O1s of pDA@PVDF (D), TiO_2-pDA@PVDF (E), and MMO-MIM (F). The O1s peak of pDA@PVDF with two typical peaks (C-OH and C=O) are corresponding to the groups in pure pDA.[24,52,53] For Figure 3E, three curves located at 529.6 eV (Ti-O-Ti), 531.3 eV (C=O/C-O ⋯Ti) and 532.2 eV (Ti-OH) can be obtained, which suggest the successful conduction of the hydrolysis process of ammonium fluotitanate on the surface of pDA@PVDF.[47,48,50] In Figure 3F, only two curves of Si-O and C-O can be obtained, which demonstrates the complete coating of imprinting layer on the surface of PVDF membrane based on the sol-gel imprinting process in the presence of TEOS and APTES (Figure 1).

As depicted in Figure 4, the morphological evolutions of the pristine PVDF membrane (A-B), pDA@PVDF (C-D), TiO_2-pDA@PVDF (E-F), and MMO-MIM (G-H) are analyzed by SEM. When comparing the pristine PVDF membrane and pDA@PVDF, the smooth and porous surfaces of pristine PVDF membrane become rough after the dopamine self-polymerization modification at a weak alkaline pH condition, which is attributed to the coating of pDA layers on the top surface of PVDF membrane. This result consists with the above-mentioned result of XPS test which can further verify the pDA modification effect. In Figure 4E-4F, the TiO_2 layers composing of abundant nano-sized TiO_2 can be observed on the surface of TiO_2-pDA@PVDF. And the much denser and apparent surface morphology of the nano-sized TiO_2 layers on the surface of PVDF membranes is obtained because of the hydrolysis of ammonium fluotitanate. As to the MMO-MIM (Figure4G-4H), the relatively diminished pore size and much rougher surfaces can be obtained after the surface-initiated sol-gel imprinted procedure on the surface TiO_2-pDA@PVDF, suggesting the readily polymerization of MIPs on the PVDF surfaces.

Optimization of preparation conditions

In this work, to obtain the optimized recognition performance of the as-prepared MMO-MIM, the impacts of different synthesis conditions such as the hydrolysis time of ammonium fluotitanate, the concentrations of template molecules, the imprinted procedure of surface-initiated sol-gel

polymerization, and washing time were investigated in detail. In addition, in order to reduce error and increase measurement precision, the fixed factors like adsorption concentration of m-cresol (600 mg L^{-1}) and adsorption temperature (25 ^{o}C) were used as the constant adsorption conditions in the whole optimized experiments.

To evaluate the influence of the hydrolysis time of ammonium fluotitanate, during the MMO-MIM synthesis, 0.5 mmol m-cresol, 0.2 mL APTES, 0.8 mL TEOS and different hydrolysis time of ammonium fluotitanate (0, 15, 30, 90, 120 min) were chosen to study. As depicted in Figure 5A, the binding capacities of MMO-MIMs enhanced with increasing the hydrolysis time of ammonium fluotitanate until 60 min, it may originate from the formation of the increasing thickness of nano-sized TiO_2 layers onto the surfaces of MMO-MIMs, which provided a more and more efficient surfaces and enhanced the adsorption ability of the as-prepared MMO-MIM during the imprinted process. Meanwhile, an obvious reduction of binding capacities for MMO-MIM could be observed after 60 min, we assume that, as the hydrolysis time increased, the overthickness of nano-sized TiO_2 layers may blocked the membrane surfaces and caused the decrease of effective surface area of membranes, which led the less formation of site accessibility during the imprinting process. Therefore, the optimized point of ammonium fluotitanate hydrolysis time at 60 min was obtained. Interestingly, as shown, when the MMO-MIM was synthetized without the surface hydrolysis action of ammonium fluotitanate (ammonium fluotitanate hydrolysis time is 0 min), the as-prepared MMO-MIM exhibited a much smaller binding capacity than that of other membranes, suggesting the signification effects of nano-sized TiO_2 modified layers for the fabrication of MMO-MIM. As a result, the nano-sized TiO_2 modified surfaces could provide homogenously distribution and bio-adhesive environment for further synthesis, directing the uniform distribution of imprinted cavities onto the surface of MMO-MIM.

In order to get the optimized synthesis concentration of templates in the preparation of MMO-MIM, batch mode operations were performed with different concentrations of m-cresol (ranging from 0.1 to 0.9 mmol), while the other synthesis conditions were remaining unchanged. As shown in Figure 5B, the binding capacities of MMO-MIMs enhanced with increase of m-cresol concentrations which could be due to the creation of more and more imprinted cavities. However, when the m-cresol concentrations were more than 0.5 mmol, a little decrease in the adsorption amount could be observed. It should be attributed to the impact and interaction

between templates at the higher concentrations of m-cresol in the process of MMO-MIM fabrication and may cause the decrease of valid recognition sites. As a result, it could be observed that a maximum amount of adsorption at the m-cresol amount of 0.5mmol was obtained.

Similarly, the impact of the surface-initiated sol-gel procedure was studied ranging from 4 to 20 h, and the experimental results were described in Figure 5C. A maximum binding capacity of MMO-MIM could be observed in the polymerization time of 12 h. The adsorption capacities of MMO-MIMs began to decrease when the polymerization time was above the turning point of 12 h. As the imprinted procedure was continued, the thicker and thicker imprinted polymer layer could be found onto the surface of MMO-MIM, which might block the template molecules to get through deeply into the imprinted layers and be difficult for the formation of effective recognition cavities. Therefore, the turning point of the imprinted procedure of surface-initiated sol-gel polymerization at 12 h was obtained.

Elution process is significantly important for the fabrication of molecularly imprinted materials, because it directly influences the rebinding capacity and selectivity of the as-prepared MIPs towards template molecules. In this work, a mixture of methanol and acetic acid (95:5, v/v) was used as an eluent to extract m-cresol from the imprinted layers on the surface of MMO-MIM. With the extraction process is going on, more and more template molecules were extracted from the MMO-MIM, leaving an increasing number of recognition cavities which were all spatially complementary of m-cresol molecule. As seen in Figure 5D, the rebinding capacities of MMO-MIMs reached the maximum value at the washing time of 8 h. What's more, as the washing time is extending, a little reduction of binding amount of m-cresol was observed. We assumed that the imprinted cavities in the imprinted layers may be partially destroyed during the elution process.

Anti-fouling performance of different synthesized membranes

To investigate the anti-fouling performance of different modified membranes, the static and dynamic BSA adsorption experiments were performed in detail. As depicted in Figure 6, the pristine PVDF membrane presented a BSA adsorption capacity of nearly 47 μg cm^{-2}, which was much larger than that of other hydrophilic modified, imprinted, and non-imprinted membranes, suggesting excellent anti-fouling performance of modified membranes. It is noteworthy that, the BSA adsorption amounts for pDA@PVDF and TiO_2-pDA@PVDF in static and dynamic

conditions were opposite. This abnormal phenomenon could be attributed to the competition of the adsorption ability and hydrophilicity of the nano-sized TiO_2 layers on the surface of pDA@PVDF. Under static BSA adsorption experiments, the adsorption capacities of membrane surfaces play the leading role. Attributed to the hydrolysis process of ammonium fluotitanate, the nano-sized TiO_2 layers could be bound onto the pDA@PVDF surfaces, which promoted the nonspecific adsorption of BSA onto membrane surfaces under static adsorption condition. So, the BSA adsorption amount of TiO_2-pDA@PVDF increased gradually after the hydrolysis process. Nevertheless, in dynamic fouling adsorption experiments, the running water can wash off the absorbed BSA on the hydrophilic surfaces more easily, the hydrophilicity of nano-sized TiO_2 layers provided the determining factor under dynamic fouling condition, which led the decrease of the BSA adsorption capacity for TiO_2-pDA@PVDF.

Meanwhile, as shown, the MMO-MIM and MMO-NIM were both keeping the lower BSA adsorption capacities than that of any other modified membranes, which suggested that the higher anti-fouling properties have been obtained after the surface-initiated sol-gel polymerization procedure. This attractive phenomenon may originate from the fabrication of more hydrophilic surface during the sol-gel polymerization procedure. The interesting part is that the MMO-MIM presents a little larger adsorption amount of BSA than that of MMO-NIM, which suggests that the MMO-NIM keeps a little higher anti-fouling ability. It should be originated from the inexistence of imprinted recognition sites in MMO-NIM makes a more hydrophilic surface during the sol-gel polymerization procedure. In addition, water contacting angle measurement was also done to further verify the surface hydrophilicity of various membranes in this work (Figure S5). Therefore, the multilayered structure with bio-inspired metal-organic strategy proposed in this work can effectively improve the anti-fouling property of molecularly imprinted membranes.

Binding performance and selectivity mechanism of MMO-MIM and MMO-NIM

The static adsorption experiments are accurately needed to investigate the rebinding capacities of molecularly imprinted materials. In this work, a series of batch mode operations were carried on to study the recognition mechanism of the as prepared MMO-MIM and MMO-NIM. As seen in Figure 7A, the adsorption rate of MMO-MIM was initially fast within a period of 20 min which took up nearly 90% of the equilibrium capacity, and then the adsorption equilibrium was obtained within 30 min. This result illustrated the obviously quick adsorption kinetics of template

molecules onto the MMO-MIM. As the control, it could be easily observed that that MMO-NIM exhibited a much slower adsorption rate and lower equilibrium adsorption amount than that of MMO-MIM. Compared with other studies, this fast kinetic adsorption performance may possibly originate from the highly active surface area (bio-inspired nano-sized TiO_2 layers) and the equally distributed imprinted cavities on the surface of MMO-MIM. This phenomenon also illustrated that although different binding sites were presented in both MMO-MIM and MMO-NIM, the high-affinity imprinted cavities of templates were created alone in MMO-MIM. To further study the rate-controlling mechanism, the pseudo-first-order rate equation and pseudo-second-order rate equation were used to further analyze the kinetic data (see Supporting Information, Table S1).[54]

As shown in the binding isotherms of MMO-MIM and MMO-NIM (Figure 7B), the MMO-MIM possessed a much higher binding capacity of m-cresol than that of MMO-NIM at any adsorption concentrations, which directed the successful conduction of surface-initiated sol-gel imprinted polymerization on the surface of TiO_2-pDA@PVDF. In addition, as shown in the optimization experiments, the bio-inspired nano-sized TiO_2 surface was also indeed helpful for this high binding amount during the synthetic process of MMO-MIM. Furthermore, this high binding capacity of MMO-NIM can further provide a high-efficiency selective permeation performance of templates. Likewise, to further study the adsorption performance of MMO-MIM, Langmuir isotherm adsorption model was used for fitting the experimental data to investigate the adsorption mechanism in detail (see Supporting Information, Table S2).[55,56]

Selectivity Analysis and Recognition Mechanism

It is significantly important to study the selectivity performance because it provides the specific recognition mechanism of the as-prepared MMO-MIM to template molecules. As shown in Figure 6C (inset), the selective adsorption experiments in this work were carried out using m-cresol, p-cresol, 2,4-DP as competitive compounds. Figure 7C describes the adsorption capacities of MMO-MIM or MMO-NIM for different targets with the feeding concentration of 400 mg L^{-1}. It can be obviously found that the MMO-MIM exhibit a much higher binding capacity of m-cresol than that of other similarities, indicating the fabrication of abundant specific recognition sites during the imprinted procedure, and the different imprinted effects may also be based on the structure, functional groups, and distinct sizes of template molecules. The binding amount of MMO-MIM for different targets presents the following order, m-cresol > p-cresol >

2,4-DP, and both the MMO-MIM and MMO-NIM possessed the similar rebinding amount for p-cresol and 2,4-DP. These findings, together with the adsorption isomers and kinetics of MMO-MIM towards m-cresol, clearly indicated that the as-prepared MMO-MIM could be used as an excellent molecularly imprinted material for selective recognition and separation of m-cresol.

Perm-selectivity analysis of MMO-MIM and MMO-NIM

During the surface initiated sol-gel imprinted polymerization, the binding cavities predetermined by shape and size of m-cresol molecules were obtained after the removal of m-cresol in the fixation of the linking groups. And the obtained imprinted cavities in the MMO-MIM can be used as the specific molecular channels for the further applications of the permeation experiments. Transport studies of MIMs could provide an incisive comprehension about the relationship between the arrangements of functional groups and the shape of the recognition sites in imprinting cavities. In this work, the transport performance and perm-selectivity of MMO-MIM and MMO-NIM were investigated in detail. Herein the permeation properties of MMO-MIM and MMO-NIM toward template molecules with different initial permeation concentrations (ranging from 50 to 600 mg L^{-1}) were performed to confirm the imprinted effects of MMO-MIM. As shown in Figure 8A, the transport fluxes of m-cresol through the MMO-MIMs are much higher than that of MMO-NIMs. One can reasonably speculate that the imprinted effects produced during the sol-gel imprinted procedure can form specific recognition sites of m-cresol on the MMO-MIM surfaces. Furthermore, the permeation factors $\beta_{\text{MMO-MIM/MMO-NIM}}$ were all more than 2.6 in the whole permeation experiments, clearly demonstrating the presence of "specific recognition sites" in the MMO-MIM. It should be mainly because that the non-formation of imprinted cavities in MMO-NIM, so non-imprinting effects could be achieved by MMO-NIM in the permeation experiments.

To further confirm the existence of the imprinted effects, the perm-selectivity performance of MMO-MIM was studied in detail. Time-dependent perm-selectivity experiments were carried out using m-cresol, p-cresol, and 2,4-DP as competitive transport molecules. The time-dependent perm-selectivity curves of MMO-MIM and MMO-NIM are shown in Figure 8b and 8c, and the permeability coefficients of m-cresol, p-cresol, and 2,4-DP through MMO-MIM and MMO-NIM are summarized in Table 1. As shown in Figure 8B, the MMO-MIM possessed a much faster permeation flux of m-cresol than that of other competitive substances, which should be mainly

attributed to the presence of sterically complementary imprinting cavities of templates (m-cresol) that hindered the transport of template molecules via binding/desorption onto the nano-sized TiO_2-pDA-based imprinted sites on the surface of MMO-MIM. The functional and spatial complementary cavities enable the template molecules transfer through the MMO-MIM in a rapid continuous way. While the other substances p-cresol, 2,4-DP presented no specific interactions with MMO-MIM, thus hindering transport by the micropore structure of membranes ("fixed carrier" membrane). On the other hand, by comparing Figure 8B with Figure 8C, a contrary permeation performance could be observed in MMO-NIM. As shown, the MMO-NIM exhibited nearly the same transport performance of m-cresol, p-cresol and 2,4-DP, which suggested that no recognition cavities were fabricated in MMO-NIM during the sol-gel polymerization without the addition of template molecules. So, the random arrangement of the functional groups of APTES in MMO-NIM resulted in no imprinting and specific recognition effects.

Besides sieving, The perm-selectivity mechanism of molecularly imprinted membrane materials can be summarized as two diametrically opposite mechanisms (retarded permeation and facilitated permeation).[34] (i) Facilitated permeation driven by preferential sorption of the template together with the better diffusion path availability (no or slower transport of non-specific solutes).[57] (ii) Retarded permeation due to affinity binding (no or slower transport of the template). Transport of templates are retarded either by binding or binding/desorption to imprinting cavities in MIMs, while another substrate which has no specific interactions with the recognition sites in imprinted membranes will be transported by diffusion or convection (membrane adsorber).[58] In this work, as depicted in the time-dependent perm-selectivity experiments, the first mechanism (facilitated permeation) played the main role in the selective separation of m-cresol. M-cresol molecules were firstly approached and adsorbed onto the imprinted cavities on the surface of MMO-MIM, and then the transport of m-cresol molecules driven by a concentration gradient is facilitated via binding/desorption to the neighbour imprinted cavities, while m-cresol molecules could transport straightforwardly through the MMO-MIM with less resistance. On the contrary, non-specific transports of p-cresol and 2,4-DP molecules are hindered by the imprinted polymer layers and micropore structure of membranes. The selective separation mechanism is diagrammatically stated in Figure 9. Furthermore, in order to obtain a deeper understanding about the perm-selectivity isomers of the as-prepared MMO-MIM, the isothermal perm-selectivity

experiments were also carried out by ranging the feeding concentrations of m-cresol and 2,4-DP from 50 to 600 mg L^{-1}. As evidenced in Figure 8D, it can be easily seen that the MMO-MIM possessed a much higher perm-selectivity property of m-cresol than that of 2,4-DP at any permeation concentrations, which directed the successful fabrication of a great number of imprinted sites in the MMO-MIM during the imprinted procedure. Furthermore, the permeation factors $\beta_{\text{m-cresol/2,4-DP}}$ were all more than 4.0 in the whole isothermal perm-selectivity experiments, which fully illustrated the presence of abundant specific recognition sites in the as-prepared MMO-MIM. In addition, the excellent regeneration ability and durability of the as-prepared MMO-MIM were achieved in this work. As depicted in Figure S6, after five adsorption/desorption cycles, the MMO-MIM could still possessed effective rebinding capacities with only 5.99% decrease of the maximum adsorption capacity.

Conclusions

In summary, for the first time, a bio-functionalized multilayered metal-organic composite methodology is proposed for the bio-inspired synthesis of molecularly imprinted nanocomposite membrane. A novel metal-organic composite structure was achieved firstly by a dopamine self-polymerization process, followed by a hydrolysis of ammonium fluotitanate on the surface of PVDF membrane. Attributing to the formation of "bio-glue" pDA layers, uniformly dispersed and tightly bound nano-sized TiO_2 layers could be formed onto the membrane surfaces. And then a surface-initiated sol-gel imprinted process was conducted on the bio-functionalized system, directing the fabrication of the multi-component metal-organic nanocomposite imprinted membrane (MMO-MIM) capable of specifically recognizing and separating m-cresol. The multilayered structure of MMO-MIM was further proved by the characterization results of ATR-FTIR, XPS, and SEM. Importantly and interestingly, through the formation of the pDA-based nano-sized TiO_2 layers, the anti-fouling performance and adsorption capacity of MMO-MIM has been remarkably improved. More importantly, we also noticed that, the as-prepared MMO-MIM possessed excellent anti-fouling property, enhanced binding capacity and highly selective separation performance as compared to those of traditional MIPs systems. The saturated adsorption capacity of MMO-MIM is 18.53 mg g^{-1}, which is about three times higher

than that of MMO-NIM (6.15 mg g^{-1}). And attributed to the unique multilayered metal-organic methodology, the enhanced perm-selectivity performances ($\beta_{MMO\text{-}MIM/MMO\text{-}NIM}$ and $\beta_{m\text{-}cresol/2,4\text{-}DP}$ are higher than 2.6 and 4.0, respectively) of MMO-MIM were obtained. Finally, this research not only provides insight into the selective recognition and separation behaviors of templates but also offers a new methodology for creating bio-functionalized multilayered metal-organic nanocomposite which is environmental friendly for scaling up without pollution.

Acknowledgments

This work was financially supported by the National Natural Science Foundation of China (Nos. 21207051, 21406085), Ph.D. Programs Foundation of Ministry of Education of China (No. 20123227120015) and Natural Science Foundation of Jiangsu Province (BK20140580), and Special Financial Grant from the China Postdoctoral Science Foundation (2014T70488).

References:

[1] M. Ulbricht, *Polymer*, 2006, **47**, 2217.

[2] M. Carta, R. Maplass-Evans, M. Croad, Y. Rogan, J. C. Jansen, P. Berardo, F. Bazzarelli, N. B. McKeown, *Science*, 2013, **339**, 303.

[3] W. Li, J. Y. Walz, *Sci. Rep.*, 2014, **4**, 4418.

[4] A. Figoli, T. Marino, S. Simone, E. D. Nicolo, X. M. Li, T. He, S. Tornaghi, E. Drioli, *Green Chem.*, 2014, **16**, 4034.

[5] W. Z. Lang, Z. L. Xu, H. Yang, W. Tong, *J. Membr. Sci.*, 2007, **288**, 123.

[6] F. Edwie, M. M. Teoh, T. S. Chung, *Chem. Eng. Sci.*, 2012, **68**, 567.

[7] J. F. Kim, G. Szekely, I. B. Valtcheva, A. G. Livingston, *Green Chem.*, 2014, **16**, 133.

[8] X. Cao, J. Ma, Z. Shi, Z. Ren, *Appl. Surf. Sci.*, 2006, **253**, 2003.

[9] L. Shao, X. Cheng, Z. Wang, J. Ma, Z.Guo, *J. Membr. Sci.*, 2014, **452**, 82.

[10] F. Liu, B. K. Zhu, Y. Y. Xu, *Appl. Surf. Sci.*, 2006, **253**, 2096.

[11] A. Ranhimpour, S. S. Madaeni, S. Zereshki, Y.Mansourpanah, *Appl. Surf. Sci.*, 2009, **255**, 7455.

[12] S. Kaur,; Z. Ma, R. Gopal, G. Singh, S. Ramakrishna, T. Matsuura, *Langmuir*, 2007, **23**, 13085.

[13] R. A. Damodar, S. J. You, H. H. Chou, *J. Hazard. Mater.*, 2009, **172**, 1321.

[14] J. H. Li, Y. Y. Xu, L. P. Zhu, J. H.Wang, C. H. Du, *J. Membr. Sci.*, 2009, **326**, 659.

[15] Y. T. Xiao, S. S. Xu, Y. C. Du, Q. S. Fu, *J. Inorg. Mater.*, 2011, **26**, 337.

[16] J. C. Love, L. A. Estroff, J. K. Kriebel, R. G. Nuzzo, G. M. Whitesides, *Chem. Rev.*, 2005, **105**, 1103.

[17] H. Lee, S. M. Dellatore, W. M. Miller, P. B. Messersmith, *Science*, 2007, **318**, 426.

[18] W. P. Liu, Y. F. Li, X. X. Meng, G. H. Liu, S. Hu, F. S. Pan, H. Wu, Z. Y. Jiang, B. Y. Wang, Z. X. Li, X. Z. Cao, *J. Mater. Chem. A*, 2013, **1**, 3713.

[19] C. Cheng, S. Li, W. F. Zhao, Q. Wei, S. Q. Nie, S. D. Sun, C. S. Zhao, *J. Membr. Sci.* 2012, **417**, 228.

[20] C. Cheng, S. Q. Nie, S. Li, H. Peng, H. Yang, L. Ma, S. D. Sun, C. S. Zhao, *J. Mater. Chem. B*, 2013, **1**, 265.

[21] L. Ma, H. Qin, C. Cheng, Y. Xia, C. He, C. X. Nie, L. R. Wang, C. S. Zhao, *J. Mater. Chem.*

B, 2014, **2**, 363,

[22] H. C. Yang, K. J. Liao, H. Huang, Q. Y. Wu, L. S. Wan, Z. K. Xu, *J. Mater. Chem. A*, 2014, **2**, 10225.

[23] H. Lee, Y. Lee, A. R. Statz, J. Rho, T. G. Park, P. B. Messersmith, *Adv. Mater.*, 2008, **20**, 1619.

[24] Q. Liu, N. Y. Wang, J. Caro, A. S. Huang, *J. Am. Chem. Soc.*, 2013, **135**, 17679.

[25] M. Zhang, X. Zhang, X. He, L. Chen, Y. Zhang, *Nanoscale*, 2012, **4**, 3141.

[26] D. H. Kim, H. J. Lee, J. M. Nam, A. Levchenko, *Adv. Mater.*, 2010, **22**, 4551.

[27] B. D. McCloskey, H. B. Park, H. Ju, B. W. Rowe, D. J. Miller, B. J. Chun, K. Kin, B. D. Freeman, *Polymer*, 2010, **51**, 3472.

[28] S. Kasemset, A. Lee, D. J. Miller, B. D. Freeman, M. M. Sharma, *J. Membr. Sci.*, 2013, **425**, 208.

[29] J. Jiang, L. Zhu, B. Zhu, Y. Xu, *Langmuir*, 2011, **27**, 14180.

[30] C. G. Xie, H. F. Li, S. Q. Li, J. Wu, Z. P. Zhang, *Anal. Chem.*, 2010, **82**, 241.

[31] G. D áz-D áz, Y. Diñeiro, M. I. Menéndez, M. C. Blanco-López, M. J. Lobo-Castañón, A. J. Miranda-Ordieres, P. Tuñón-Blanco, *Polymer*, 2011, **52**, 2468.

[32] B. Y. Huang, Y. C. Chen, G. R. Wang, C. Y. Liu, *J. Chromatogr. A*, 2011, **1218**, 849.

[33] A. T. Larsen, T. Lai, V. Polic, K. Auclair, *Green Chem.*, 2012, **14**, 2206.

[34] M. Ulbricht, *J. Chromatogr. B*, 2004, **804**, 113.

[35] Y. L. Wu, M. Yan, Y. S. Yan, X. L. Liu, M. J. Meng, P. Lv, J. M. Pan, P. W. Huo, C. X. Li, *Langmuir*, 2014, **30**, 14789.

[36] G. Szekely, I. B. Valtcheva, J. F. Kim, A. G. Livingston, *J. Membr. Sci.*, 2015, **86**, 215.

[37] M. M. Moein, A. EI-Beqqali, M. Javanbakht, M. Karimi, B. Akbari-adergani, M. Abdel-Rehim, *J. Chromatogr. A*, 2014, **1372**, 55.

[38] Y. T. Wu, Y. H. Zhang, M. Zhang, F. Liu, Y. C. Wan, Z. Huang, L. Ye, Q. Zhou, Y. Shi, B. Lu, *Food Chem.*, 2014, **164**, 527.

[39] J. A. Young, *J. Chem. Educ.*, 2006, **83**, 1753.

[40] D. Rajkumar, K. Palanivelu, *Ind. Eng. Chem. Res.*, 2003, **42**, 1833.

[41] L. S. Richard, C. E. S. Bernardes, H. P. Diogo, J. P. Leal, M. E. Minas da Piedade, *J. Phys. Chem. A.*, 2007, **111**, 8741.

[42] W. H. Hatcher, F. W. Skirrow, *J. Phys. Chem. A.*, 1917, **39**, 1939.

[43] H. P. Meissner, Jr. F. E. French, *J. Am. Chem. Soc.*, 1952, **74**, 1000.

[44] S. J. Liu, X. M. Liu, C. Wang, *Ind. Eng. Chem. Res.*, 2013, **52**, 16719.

[45] R. C. Huston, P. S. Chen, *J. Am. Chem. Soc.*, 1933, **55**, 4214.

[46] S. L. Whittenburg, S. J. McKinnon, V. K. Jain, R. F. Evilia, *J. Phys. Chem.*, 1988, **92**, 4236.

[47] L. Ge, M. Xu, *J. Sol-Gel Sci. Technol.*, 2007, **43**, 1.

[48] H. Choi, A. C. Sofranko, D. D. Dionysiou, *Adv. Funct. Mater.*, 2006, **16**, 1067.

[49] Y. Suda, H. Kawasaki, T. Ueda, T. Ohshima, *Thin Solid Films*, 2004, **453**, 162.

[50] C. Chen, M. C. Long, H. Zeng, W. M. Cai, B. X. Zhou, J. Y. Zhang, Y. H. Wu, D. W. Ding, D. Y. Wu, *J. Mol. Catal. A: Chem.*, 2009, **314**, 35.

[51] L. Shao, S. Quan, Y. Liu, Z. H. Guo, Z. X. Wang, *Mater. Lett.*, **2013**, 107, 307.

[52] J. Ou, J. Wang, D. Zhang, P. Zhang, S. Liu, P. Yan, B. Liu, S. Yang, *Colloid. Surface. B*, 2010, **76**, 123.

[53] P. Zhang, C. Shao, Z. Zhang, M. Zhang, J. Mu, Z. Guo, Y. Liu, *Nanoscale*, 2011, **3**, 2943.

[54] I. Langmuir, *J. Am. Chem. Soc.*, 1918, **40**, 1361.

[55] Y. S. Ho, G. McKay, *WaterRes.*, 1999, **33**, 578.

[56] Y. S. Ho, G. McKay, *Process Biochem.*, 1999, **34**, 451.

[57] D. K. Roper, E. N. Lightfoot, *J. Chromatogr. A*, 1995, **702**, 3.

[58] R. D. Noble, *J. Membr. Sci.*, 1992, **75**, 121.

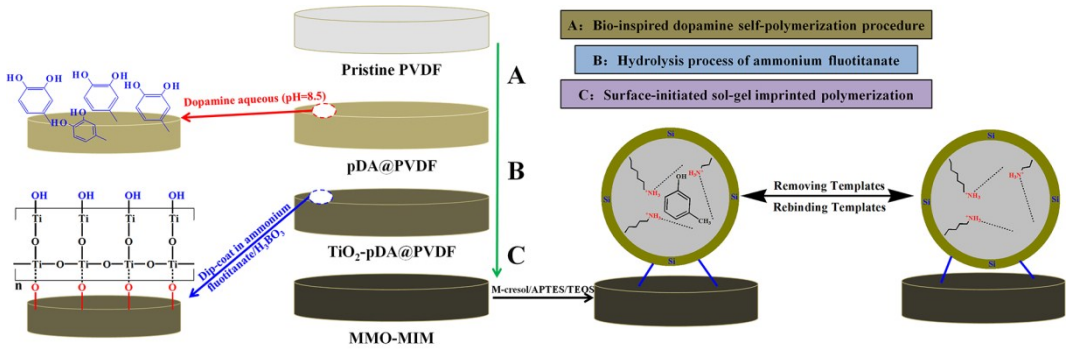

Figure 1. The schematic methodology and possible mechanisms for the bio-inspired synthesis of MMO-MIM with multilayered metal-organic nanocomposite structure.

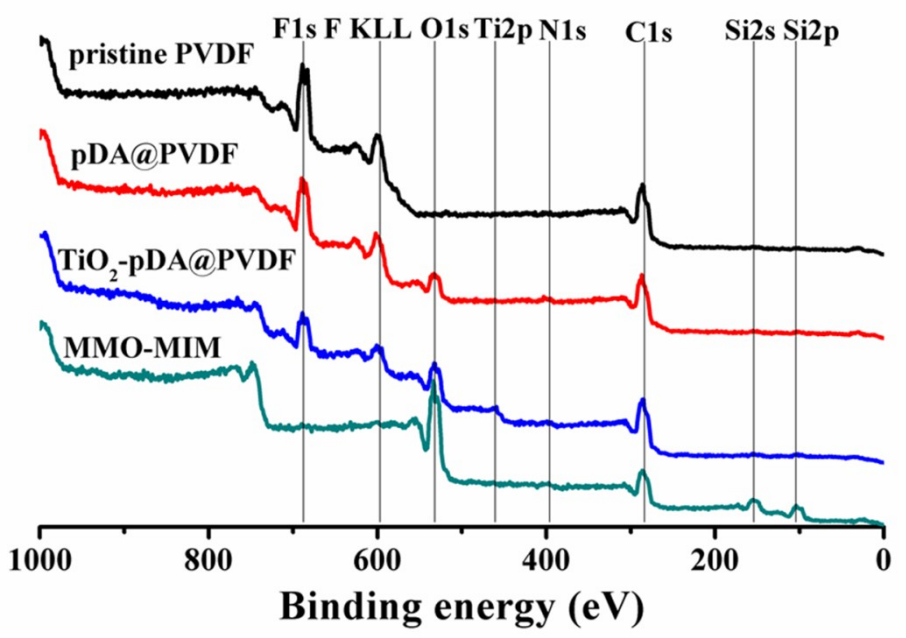

Figure 2. X-ray photoelectron spectroscopy (XPS) wide scan of pristine PVDF membrane, pDA@PVDF membrane, TiO_2-pDA@PVDF, and MMO-MIM.

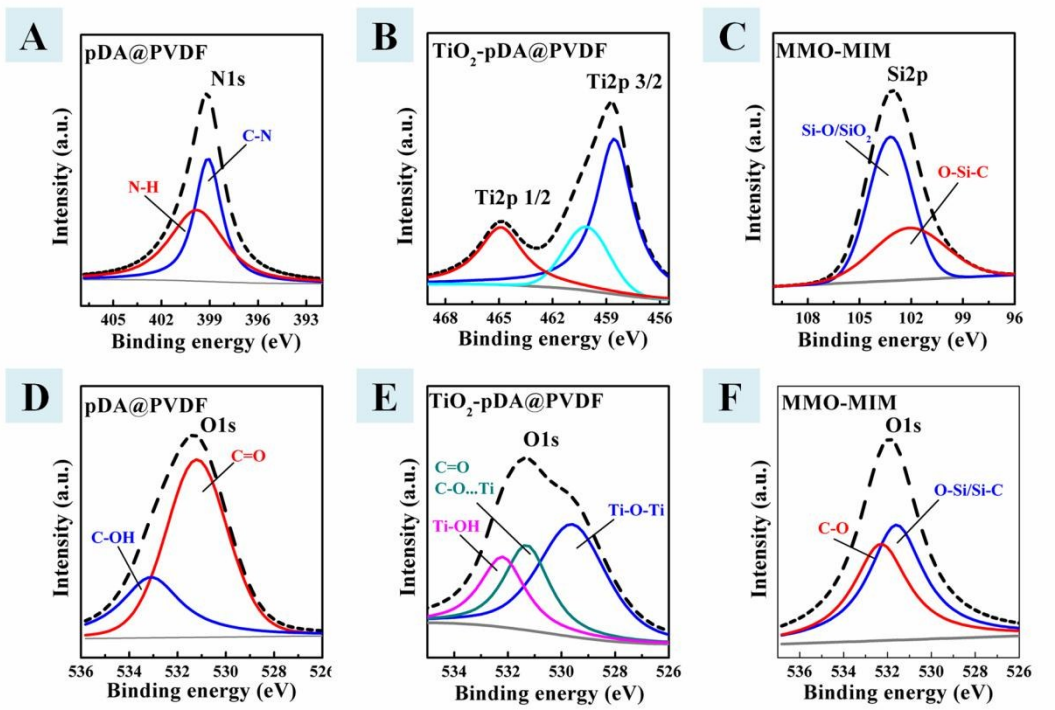

Figure 3. XPS curve-fitting results of N1s (A), Ti2p (B), Si2p (C), and O1s (D-F).

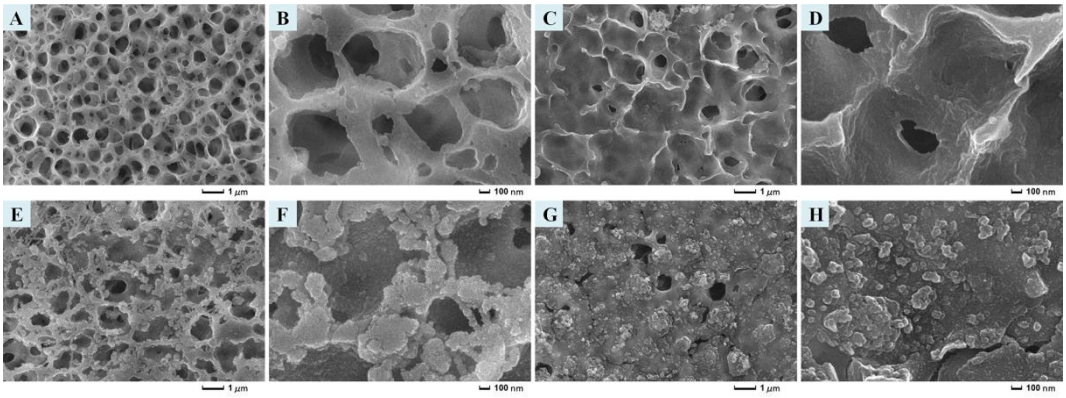

Figure 4. Surface microstructures of: (A-B) pristine PVDF membrane, (C-D) pDA@PVDF membrane, (E-F) TiO_2-pDA@PVDF membrane, (G-H) MMO-MIM.

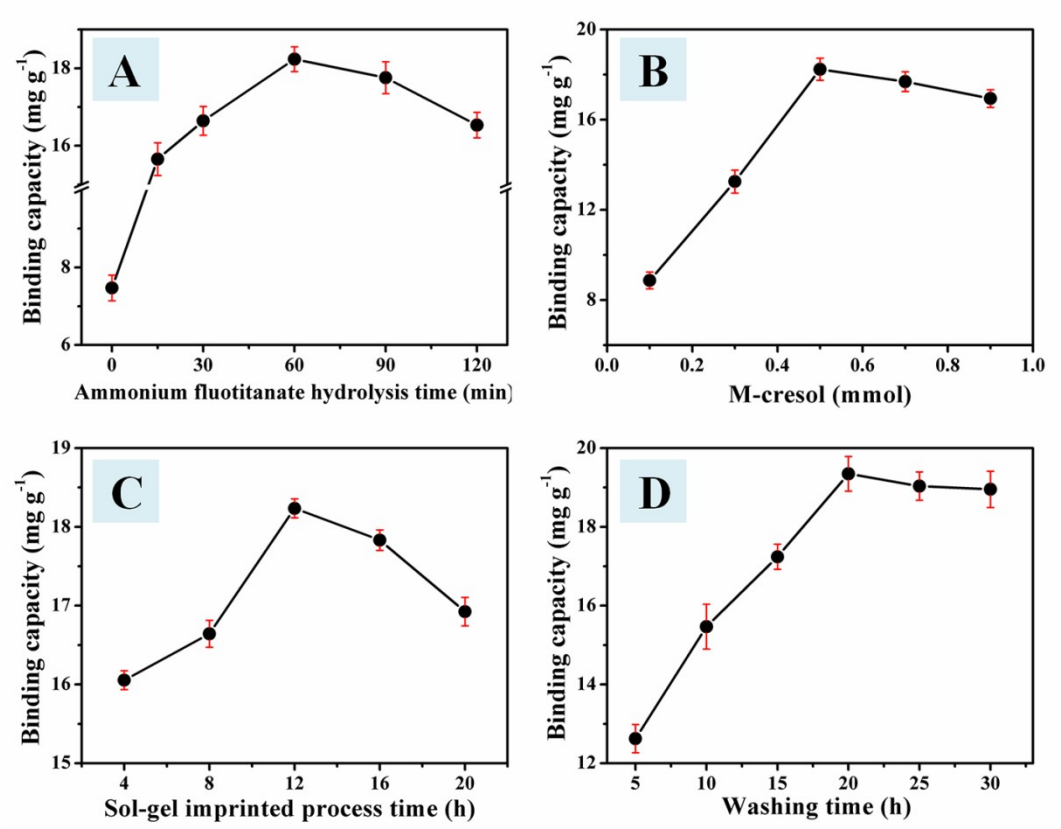

Figure 5. Effects of (A) the hydrolysis time of ammonium fluotitanate, (B) amount of template molecules, (C) polymerization time of the surface-initiated sol-gel imprinted procedure, and (D) washing time on the binding capacities of MMO-MIM.

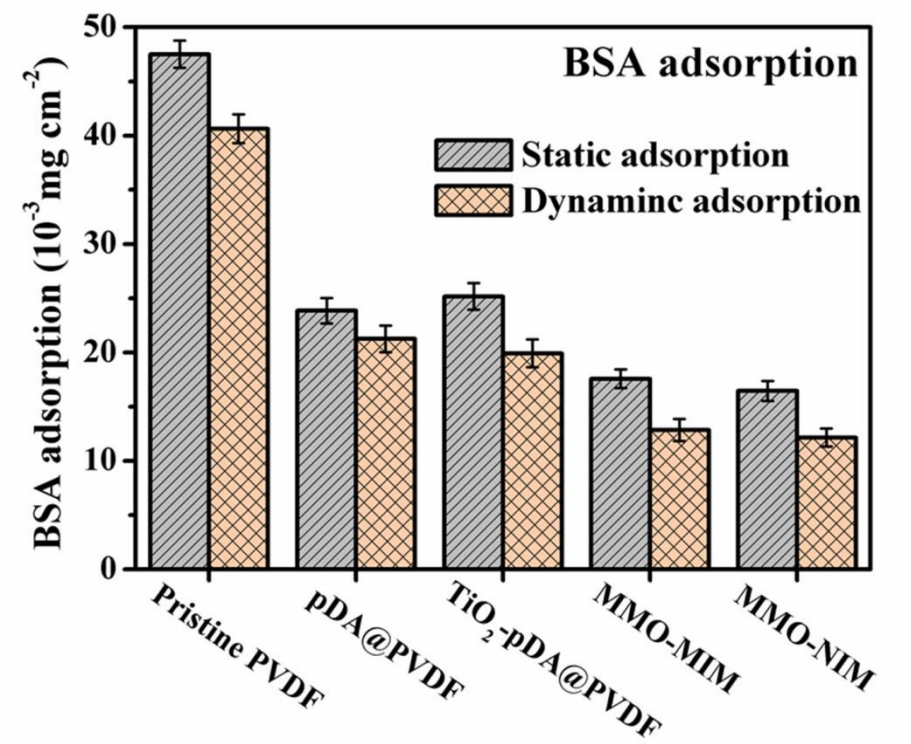

Figure 6. BSA adsorption behaviors onto various membranes measured under static and dynamic conditions.

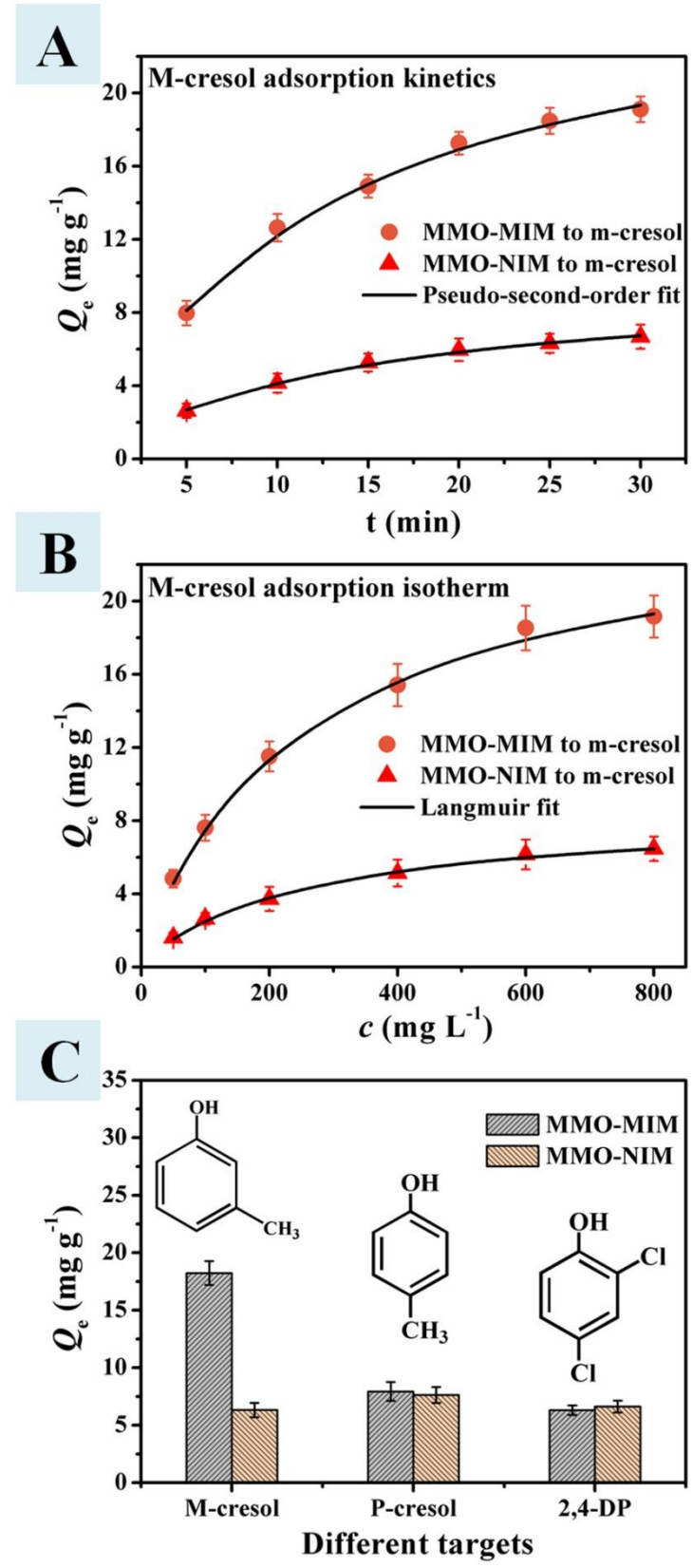

Figure 7. (A) Kinetic data and modeling for the adsorption of m-cresol onto MMO-MIM and MMO-NIM, (B) Adsorption isotherms of m-cresol onto MMO-MIM and MMO-NIM with the

fitting to Langmuir model, (C) Selective binding cavities of MMO-MIM and MMO-NIM for different targets (inset are the molecular structure of test compounds).

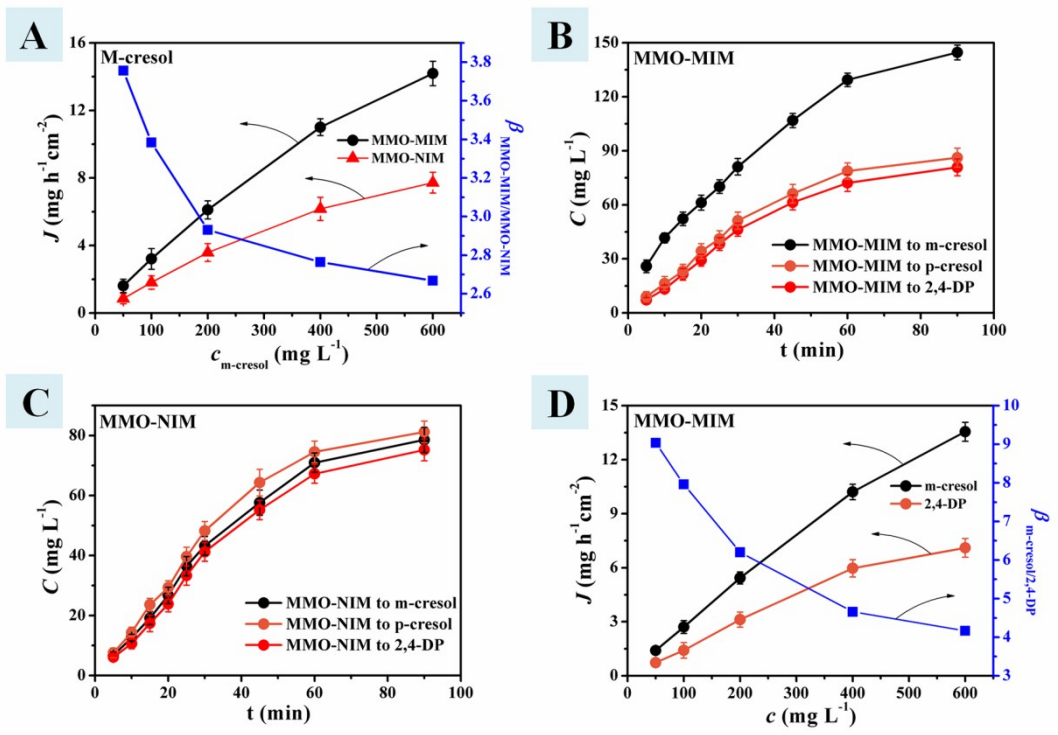

Figure 8. (A) Static transport performances of MMO-MIM and MMO-NIM toward m-cresol, time-dependent perm-selectivity curves of m-cresol, p-cresol, and 2,4-DP through MMO-MIM (B) and MMO-NIM (C), perm-selectivity isotherms (D) of m-cresol and 2,4-DP through the MMO-MIM and the calculated $\beta_{\text{m-cresol/2,4-DP}}$ values.

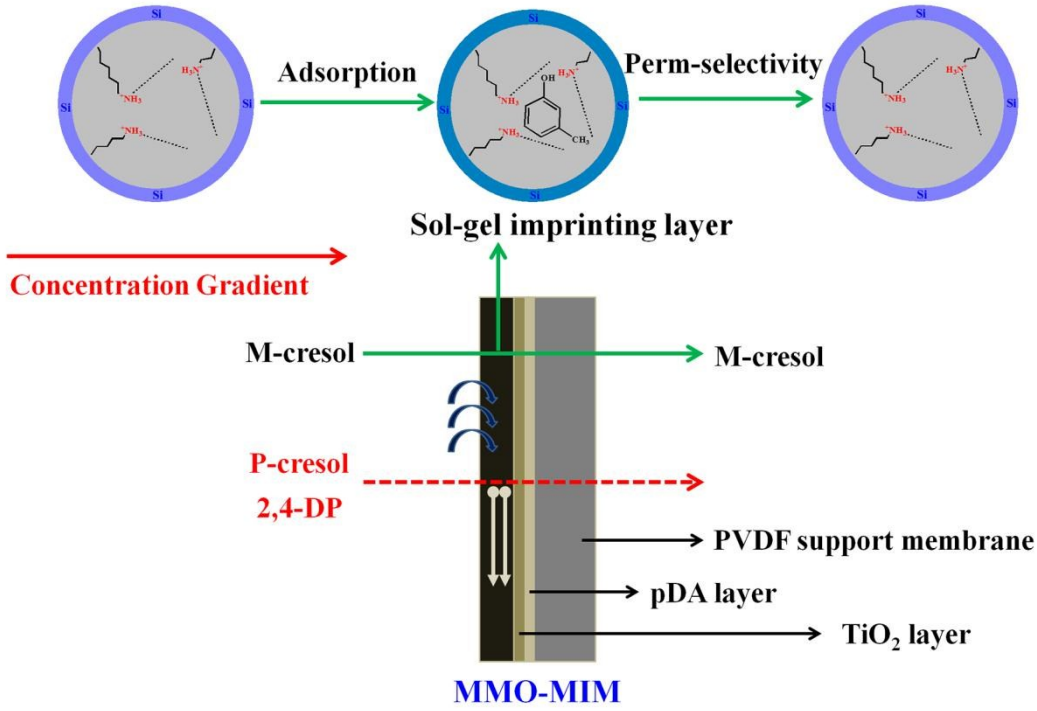

Figure 9. Schematic representation of the temperature-dependent permeation performances of MMO-MIM.

Table 1. Time-permeation results (after 60 min) of MMO-MIM and MMO-NIM for m-cresol, p-cresol, 2,4-DP (the data are the mean of at least three independent experiments).

Membranes	Substrates	J ($mgcm^{-2}h^{-1}$)	P (cm^2h^{-1})	$\beta_{m\text{-}cresol/p\text{-}cresol}$	$\beta_{m\text{-}cresol/2,4\text{-}DP}$
MMO-MIM	m-cresol	8.19	58.05	3.52	4.09
	p-cresol	4.67	16.49		
	2,4-DP	3.99	14.21		
MMO-NIM	m-cresol	4.49	17.42	0.93	1.09
	p-cresol	4.72	18.81		
	2,4-DP	4.26	16.04		

Table of Contents

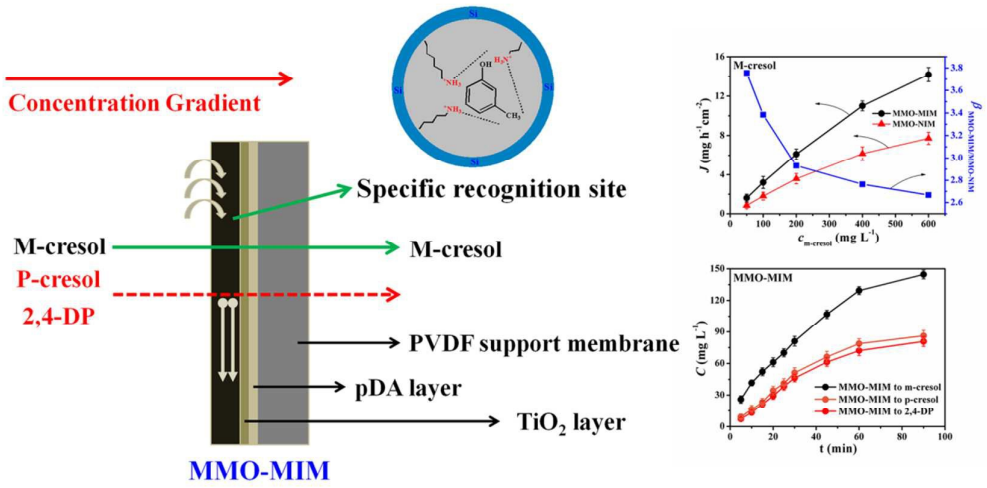

Bio-inspired multi-component metal-organic nanocomposite imprinted membranes capable of selective recognizing and separating m-cresol molecules have been prepared.